

## Application of DRP scheme solving for rotating disk-driven cavity

Reui-Kuo Lin<sup>1,\*</sup>, Shun-Feng Tsai<sup>2</sup>, Kwan Ouyang<sup>3</sup>

1, Department of Marine Engineering, Taipei College of Maritime Technology, No. 212, Sec. 9, Yen Ping N. Rd., Shihlin Dist., Taipei 11174, Taiwan, Republic of China (R.O.C)

2, Department of Marine Engineering, National Taiwan Ocean University, No.2, Beining Rd., Zhongzheng District, Keelung City 202, Taiwan, Republic of China (R.O.C)

3, Department of Marine Engineering, Taipei College of Maritime Technology, No. 212, Sec. 9, Yen Ping N. Rd., Shihlin Dist., Taipei 11174, Taiwan, Republic of China (R.O.C)

\* Correspondent, Assistant Professor; TEL: 886-2-28102292-5023;

### ABSTRACT:

This paper is to explore when the rotating disk-driven cube container structure flow generated by different Reynolds numbers to observe structural reasons and swirl flow field generated in the space discretization dispersion-relation-preserving (DRP) scheme finite difference method, time item then use total variation diminishing (TVD) Runge-Kutta method format, thereby to achieve the accuracy of its value, the paper also use topological theory to analyze the characteristics of singularity, and draw a three-dimensional flow field pattern thereby to observe the structure and flow of the flow field case, with the result that the Reynolds number increased flow into the spiral point position will gradually close the bottom of the cavity, and with the impact of an increase in the Reynolds number at the bottom of the singular point significantly smaller.

**Keywords:** disk-driven, Reynolds number, dispersion-relation-preserving (DRP), total variation diminishing (TVD), Runge-Kutta, topological theory

### I. INTRODUCTION

Because the relationship between today's emphases on efficiency, with essays program to deal with less fluid flow analysis, the majority are based software package for simulation analysis. However, due to physical problems, there are many possibilities and variations, this paper attempts to analyze essays program flow structure in the disk-driven under the influence of the cube.

In the past the process industries often use to drive the rotating disk-driven flow cylinder, rectangular, or cube thereby to understand the internal structure of the fluid flow. Applying a simple geometric structure of the flow field to explore rotation can help analyze and understand the principles of early and recent research literature mostly cylindrical or rectangular shape, so this article is to explore the use of a cube shape, in their daily lives the most common is the computer's CD-ROM drive, using a rotary disc pieces to bring the whole flow field, hoping to apply the same theory to understand the internal structure of the rotating disk-driven flow, the paper is a continuation of the literature Chiang et al. study [11] was made to continue. To investigate the flow structure when  $Re > 2000$  after arising.

Benjamin and Denny [1] with the vorticity-stream function method to simulate the two-dimensional closed pull hole course and supplemented with multi-grid method, will increase the numerical simulation of the Reynolds number to 104, expressly found that the two-dimensional geometry of a closed pulling hole course located primary vortical center and three times the corner vortical. Koseff and Street [2] employed the experimental data for a series of studies with discussion. Koseff and Street [3] were the top three drivers pulled closed experimental observation point field, when the Reynolds number is between 6000-8000, the structure of the turbulent rotating disk-driven flow for the first time the show. Fenstermacher [4] used laser-Doppler velocimetry explore concentric circles in the middle of the restricted fluid flow from the column transition situations arising from the rotation. Chenoweth and Eyret [5] found that when the Reynolds number is higher than a certain value, the main component of the two-dimensional flow field in the following structure: the geometric center of the vortical in the main (primary eddy), located at the corner of the three sub-swirl (secondary eddy).

Liao et al. [6] using numerical simulation method of rotating between the cylinder when the non-denaturing conditions axisymmetric ilk, and the use of numerical methods for solving the three-dimensional Navier-Stokes equations, the accuracy of its value on having a second-order accurate in time and space, in changing Couette-Taylor flow field, Liao et al clearly parsed revolving cylinder, transitional flow conditions and the structural characteristics of the flow patterns between. Tam et al. [7] proposed to keep the format dispersion relation scheme, the use of the best ways to improve spatial discrete wave number format analog capability. We can also use its spherical shaped segments to observe the distribution of the entire three-dimensional rotating driven cavity flow. Inamuro et al. [8] use variables to calculate the angular velocity ( $R\Omega$ ), drawing plane streamlines and velocity vectors to observe the driven cavity flow.

In this paper, in order to make more accurate numerical studies, spatial discrete part of the Navier-Stokes equation literature [9] ownership dispersion-relation-pressure formulation finite difference method, at the time part of discrete items literature [10] retain TVD Runge-Kutta method and for different Reynolds number of numerical results are discussed its flow structure, and to explore the reasons for its physical phenomena and secondary flow generated.

## II. WORKING EQUATIONS

We consider in this paper the Navier-Stokes equations for velocity  $u$  and pressure  $p$  :

$$\frac{\partial u_i}{\partial t} + \frac{\partial}{\partial x_j}(u_j u_i) = -\frac{\partial p}{\partial x_i} + \frac{1}{\text{Re}} \frac{\partial^2 u_i}{\partial x_m \partial x_m} \tag{1}$$

The above equations of motion are under the constraint condition of fluid incompressibility,

$$\frac{\partial u_i}{\partial x_i} = 0 \tag{2}$$

The above two equations will be solved subject to the initial divergence-free velocity condition and boundary velocities to close the problem. In this primitive-variable formulation, specification of velocity boundary conditions has been rigorously proven [11]. For this study, we concentrate to steady and laminar conditions. The Reynolds number  $\text{Re}$  is defined by choosing the maximum rotation speed of the disk ( $R\Omega$ ) as the characteristic speed and the radius of the rotating disk ( $R$ ) as the characteristic length. In this study, the pressure has been normalized by  $p(R^2\Omega^2)$  where  $\Omega$  denotes the angular velocity of the disk.

The rationale behind adopting the velocity -pressure formulation is that it provides closure boundary conditions [8], Referring to Figure 1, no-slip boundary conditions for velocities  $u_i$  are specified everywhere except at the upper wall, where a disk of radius 1 rotates with a constant value of  $\Omega$  which is referred to as the disk angular speed. No pressure boundary condition is permitted at the boundary where velocities are specified; otherwise, the investigated elliptic system will be over determined [8].

The appearance and disappearance of non-wandering set is called bifurcation. knowledge about the changes in flow stability and bifurcation, which always coincide in nonlinear dynamics, is thus crucial to get a better understanding of the currently investigated nonlinear differential system. Another main objective in conducting this study is to explore the hydrodynamic details based on the topology theory.

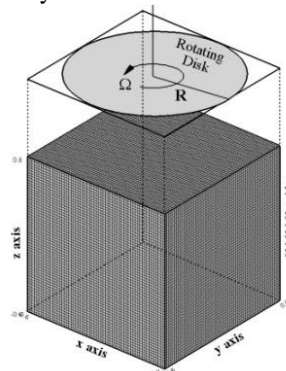


Figure 1. Description of the investigated rotating disk-driven cavity problem and the non-uniform grid distribution  $61^3$  on the bounding surfaces.

## III. FINITE DIFFERENCE METHOD

Discrete numerical methods of solving numerical simulation of rotating disk-driven flow compression is not available to the general use of discrete intermediate pressure gradient difference method detects the unreasonable pressure field, so the literature [9-10] have proposed on the same grid size position high-precision,

high-resolution compact model and can suppress the fluctuation-induced generalized principle and the principle of stability of the momentum equation to deal with the pressure gradient term, and the other according to Tam and Webb [9] proposed dispersion-relation-preserving (DRP) scheme discrete governing equations using best of space discrete method to improve the format for the wave number of simulation capabilities. Its core idea is assumed that the function  $\phi(x)$  of the Fourier transform of  $\tilde{\phi}(\alpha)$ , is  $\partial\phi/\partial x$  the Fourier transform of  $i\alpha\tilde{\phi}(\alpha)$ . The corresponding difference scheme inevitably transformed with the presence of poor guide. The DRP format to maintain a certain precision, the optimized dispersion coefficient difference can lead to a minimum.

### 3.1. Dispersion-relation-preserving advection scheme

In this paper, the advection term in the level set equation is discretized using the DRP dual-compact scheme [12], and the advection term in the momentum equation is discretized using the multi-dimensional DRP upwinding scheme [13]. The underlying idea in the DRP method is as follows: to physically predict the first derivative term accurately, the dispersive nature embedded in it must be retained as much as possible. The reason for this is that the dispersion relation governs the relationship between the angular frequency and the wavenumber of the first-order dispersive term [9]. In other words, it is possible to predict the solution accurately provided that the dispersion relation is well preserved. To achieve this, we combine the Taylor series expansion analysis with the Fourier transform analysis to derive the discretized coefficients. For details of the derivations, the interested reader is invited to refer to [12] and [13].

### 3.2. Solver in non-staggered grids

Within the context of velocity-pressure formulation, one has a choice of employing a staggering [14] or a collocating [15] grid strategy for the storage of working variables. While use of both approaches can suppress node-to-node pressure oscillations, we adopt in this study the collocating grid approach for the sake of programming simplicity. When solving the incompressible Navier-Stokes equations (1-2), two well-known numerical instabilities may be encountered in cases when the convection term dominates the diffusion term. We will employ the DRP upwinding scheme detailed in [16] to resolve this numerical instability problem.

The second computational difficulty is to assure the discrete divergence-free condition for the working velocity vector. While this constraint condition can be automatically satisfied in the approach based on a mixed formulation, a much larger algebraic system needs to be solved due to the mass conservation equation. The convergent solutions for  $(u_i, p)$ , which  $i = 1 \sim 3$ , in a domain with a large number of mesh points become much difficult to be calculated using a computationally less expensive iterative solver [17]. Derivation of a proper equation for the  $p$  replace the divergence-free equation (2) is therefore adopted in this study. This class of approaches involves using a rigorously derived integral boundary condition [18,19] and the calculation of matrix solutions becomes computationally more challenging. Due to these drawbacks, we employ in this study the fractional-step method to advance the calculation through a sequence of sub-steps.

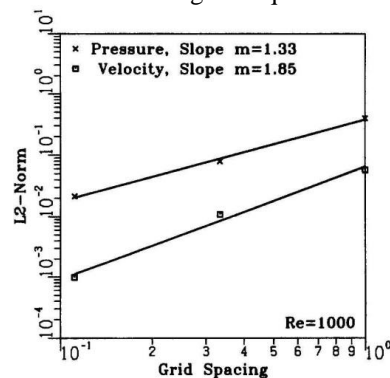


Figure 2. Rates of convergence for velocity magnitude  $(u^2+v^2+w^2)^{1/2}$  well as pressure.

### 3.3. Velocity-pressure coupling

When solving the incompressible flow equation, special care must be taken for the velocity and pressure coupling. While a staggered grid has been demonstrated to be able to eliminate the odd-even decoupling problem, the resulting programming complexity is still a key task. For our purposes, we use a semi-staggered grid to couple the velocity and pressure [20]. The velocity vectors are stored at the edge of the cell, whereas pressure and other scalar fields are stored at the center, as shown in Figure 2. The programming complexity is much lower for this grid system, compared to the staggered grid, and the coupling may be easily achieved if one employs a pressure interpolation from cell center to edge.

We have benchmarked the computer code employed here by taking the analytic velocity vector  $u(x_i, t = 0)$ , as given in the problem of Ethier and Steinman [21], the specified boundary velocities. In this study, solutions computed at the finest grid ( $h = 1/61$ ) are regarded as reference values for conducting the rate of convergence test. According to our previous work [8], the rates of convergence for velocities and pressure are plotted in Figure 2. The success in validating the analysis code provides us with strong confidence to study the driven cavity flow subjected to a rotating disk.

In this study, first chosen  $Re = 1000, 2000, 3000, 4000$  with experimental data and references each comparison and verification can clearly be seen from Figure 2, with the increase in the number of apparent speed will increase. This article draws from the numerical results of different Reynolds numbers into the speed chart, the pressure diagram, fluid flow map, vorticity map to explore several Reynolds number is not found in the structure of the flow field in the gap is too large, and so this article will explore the entire steady since the structure of the flow field.

## IV. RESULTS AND DISCUSSIONS

### 4.1. Problem description

The disk-container assembly is shown schematically in Figure 1. On the roof of the cavity, a disk of radius 1 is mounted coaxially with the centroid of the cubical cavity, which has a length of 2. This disk rotates constantly with an angular speed  $\Omega$ , driving an initially resting liquid fluid and thereby resulting in a vortical flow. For this study, we address the effect of the rotation speed, or Reynolds number as defined in Section 2, of the disk on the established vortical flow structure. We also explore into the kinematic aspect of the primary vortical flow and the secondary flow.

On the roof of the rotating disk-cavity flow, a disk of radius 1 is mounted coaxially with the centroid of the cube, which has a length of 2. This rotating disk-cavity flow constantly with an angular speed  $\Omega$ , driving an initially resting liquid fluid and thereby resulting in a vortical flow. The Reynolds number chosen for this study is defined by the lid speed, the width of the cavity, and the kinematic viscosity of the working fluid.

### 4.2. Disk-driven vortical flows

Figure 3 compares the rate for the  $z$  direction, from the figure that as the Reynolds number can increase the speed will be higher. Then from Figure 4 in the plane  $y = 0$  for four different Reynolds number flow field pattern, can be observed from the figure had one pair of swirl and eddy currents in different directions of rotation near the top center of the cavity, it is because the top a rotating disk ( $z$  direction is the angular velocity), prompting the fluid passes through the center of the chamber to flow upward, fluid particles flowing near the cavity direction downwardly into the vertical end wall, thereby forming a secondary flow structure is inverted. Different faces from Figure 5(a)  $z$  direction of the flow field, can observe all of the flow is to the middle of the stream into the boundary wall, the structure of the flow field around the rotation coupled fluid flow into the middle part caused by distortions phenomenon, in the plane  $z = 0.4$  can be observed that the four corners of the visible presence four secondary flow, because of the adverse pressure gradient caused by the occurrence of reflux, the formation of secondary flow in the four corners of the biggest reason is because effect of viscosity caused by shear stress.

From Figure 5(b) observed vorticity  $z$  direction, this flow field is a rotating flow it will generate vorticity, vorticity can be seen from the middle part of the vorticity maximum, because with the amount of rotation in the middle of both the shear stress so large relative vorticity is relatively large near the smaller boundary layer vorticity, and the greater the surface vorticity near the top of the disk. And from the speed can also explain why in the middle of the main vortical vorticity will be greater than four secondary flow vorticity. Topological theory can be obtained by the use of flow into the spiral point (attracting-spiral2d), at  $y = \pm 0.6$ ,  $x = \pm 0.6$ ,  $z = -0.6$  and  $z = +0.6$  has two faces, three-dimensional map plotted as Figure 6, from the figure can be found at the top of a counter-clockwise rotation of the disk can be used to drive the flow field, from each of the boundary wall flows into the direction of flow can be learned, when  $Re = 1000$  the entire flow field flow direction are along the flow direction of rotation of disk.

When  $Re = 3000$  when, from Figure 7 can be observed, as the Reynolds number increases speed becomes faster so the fluid flow lines are more intensive in the  $z = 0.4$  surface persistence of four secondary flow in  $z = -0.59$  surface location can be found in the direction of rotation along four distinct swirl counterclockwise also followed a slight change in the main part of the increase in the speed of the vortical near the boundary at four whirlpool reduced, and the pressure is just the opposite this also explains why the primary vortical vorticity increased four secondary flow vorticity smaller reasons. Figure 8 can be more clearly seen in the case of the speed of each plane and the flow. In Figure 9, when  $z = -0.6$ ,  $y = \pm 0.6$ ,  $x = \pm 0.6$ , to produce a

spiral flow into the point to drive the entire flow, the entire flow way and are rotating disk-driven cavity flow counterclockwise along without any change.

## V. CONCLUSIONS

This study is mainly aimed at different Reynolds number as explore its structure flow mechanism and physical behavior. Discussion In this study, the top three-dimensional rotating disk-driven cavity flow impose certain practical value of the angular velocity  $\Omega$  clockwise, we will chose  $500 \leq Re \leq 4000$ , to analyze the singularity into the spiral flow characteristics calculated for each surface point using topology theory, from three-dimensional disk-driven cavity flow can understand the situation led the whole flow. At  $500 \leq Re \leq 4000$  analysis found that the flow of the flow field is very similar, except that with the Reynolds number increases speed and pressure will change, because the speed of the flow field flow lines caused by change-intensive, but the basic structure of the flow field which no significant change in disk-driven cavity flow pattern. Topology through a singular point of theoretical calculations can be found as the Reynolds number increases to flow into the position will gradually spiral point near the bottom of the cavity, and with the impact of an increase in the Reynolds number at the bottom of the singular point significantly smaller. In the face of  $z = -0.59$  four vortical continued close to the end wall, this is because as the Reynolds number increases speed along faster, so when the speed increases viscous force it will be relatively minor role to the boundary near the end wall.

## ACKNOWLEDGEMENTS

The financial supports provided by the Ministry of Science and Technology under grants 102-2221-E-229-001 and 103-2221-E-229-002 are gratefully acknowledged. Computational hardware supports from the National Center of High-performance Computing and National Taiwan University are also highly appreciated.

## REFERENCES

- [1] X. Ruiz, M. Aguiló, J. Massons, F. Díaz. Numerical and experimental of the forced convection inside a rotating disk-cylinder configuration, *Experiments in Fluids*, 14, pp. 333-340, 1993.
- [2] E. Lang, K. Sridhar, N. W. Wilson. Computational study of disk driven rotating flow in a cylindrical enclosure, *Journal of Fluids Engineering*, 116, pp. 815-820, 1994.
- [3] H. P. Pao. Numerical solution of the Navier-Stokes equations for flows in the disk-cylinder system, *Physics of Fluids*, 15, pp. 4-11, 1972.
- [4] R. Legendre. Séparation de courant l'écoulement laminaire tridimensionnel. *Rech. Aéro*, 54, pp. 3, 1972, 1956.
- [5] M. J. Lighthill. Attachment and separation in three-dimensional flow, In *Laminar Boundary Layers*, II, ed. L. Rosenhead. Oxford University Press, 26, pp. 72-82, 1963.
- [6] Tobak Murray, D.J. Peake. Topology of three-dimensional separated flows, *Annual Review of Fluid Mechanics*, 14, pp. 61-85, 1982.
- [7] L. A. Yates, G. T. Chapman. Streamlines, vorticity lines and vortices around three-dimensional bodies, *AIAA Journal*, 30(7), pp. 1819-1826, 1992.
- [8] H. U. Vogel. Experimentelle Ergebnisse über die laminare Strömung in einem zylindrischen Gehäuse mit darin rotierender Scheibe, *MPI Bericht*, 6, 1968.
- [9] Tam K. W. Christopher, Jay C. Webb. Dispersion-relation-preserving finite difference schemes for computational acoustics, *J. Comput. Phys.*, Vol. 107: 262-281, 1993.
- [10] A. Harten, S. Osher, S. R. Chakravarthy. Uniformly high-order accurate essentially non-oscillatory schemes 3. *J. Comput. Phys.* Vol. 71: 231-303, 1987.
- [11] T. P. Chiang, W. H. Sheu, S. F. Tsai. Topological flow structure in backward-facing step channels, *Comput. Fluids*, 26(4), pp. 321-337, 1997.
- [12] P. H. Chiu, W. H. Sheu. On the development of a dispersion-relation-preserving dual-compact upwind scheme for convection-diffusion equation, *Journal of Computational Physics*, 228, pp. 3640-3655, 2009.
- [13] P. H. Chiu, W. H. Sheu, R. K. Lin. Development of a dispersion-relation-preserving upwinding scheme for incompressible Navier-Stokes equations on non-staggered grids, *Numerical Heat Transfer Part B: Fundamentals*, 48, pp. 543-569, 2005.
- [14] S. K. Lele. Compact finite difference schemes with spectral-like resolution, *Journal of Computational Physics*, 103, pp. 16-42, 1992.
- [15] S. V. Patankar. *Numerical Heat Transfer and Fluid Flow*, McGraw-Hill, New York, 1980.
- [16] S. Abdallah. Numerical solution for the incompressible Navier-Stokes equations in primitive variables using a non-staggered grid II, *Journal of Computational Physics*, 70, pp. 193-202, 1987.
- [17] M. T. Wang, W. H. Sheu. An element-by-element BICGSTAB iterative method for threedimensional steady Navier-Stokes equations, *Journal of Computational and Applied Mathematics*, 79, pp. 147-165, 1997.
- [18] L. Quartapelle, M. Napolitano. Integral conditions for the pressure in the computation of incompressible viscous flows, *Journal of Computational Physics*, 62, pp. 340-348, 1986.
- [19] P. Lin. A sequential regularization method for time-dependent incompressible Navier-Stokes equations, *SIAM J. Numer. Anal.* 34(3), pp. 1051-1071, 1997.
- [20] C. M. Rhie, W. L. Chow. A numerical study of the turbulent flow past on airfoil with trailing edge separation, *Report AIAA-82-0988*, 1982.
- [21] C. R. Ethier, D. A. Steinman. Exact full 3D Navier-Stokes solutions for benchmarking, *Int. J. Numer. Meth. in Fluids*, 19, pp. 369-375, 1994.

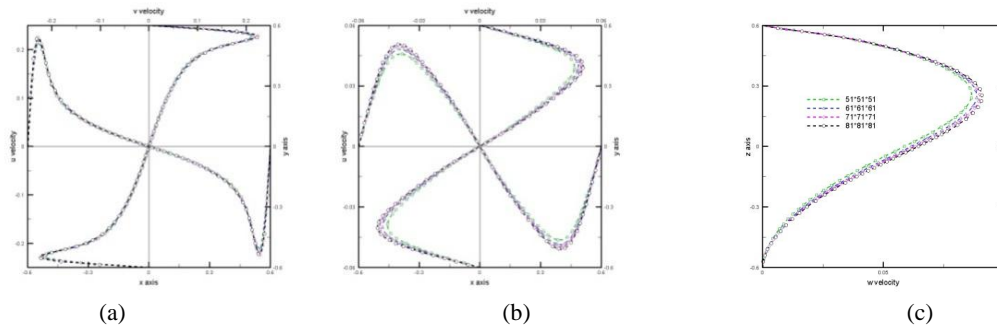


Figure 3. Grid independence tests for the problem, shown in Figure 1, with  $Re = 1000$  : (a)  $u(0, y, 0.9)$  and  $v(x, 0, 0.9)$  ; (b)  $u(0, y, 0)$  and  $v(x, 0, 0)$  ; (c)  $u(0, y, -0.9)$  and  $w(0, 0, z)$  .

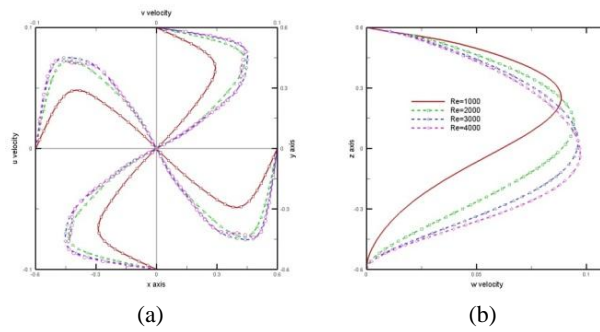


Figure 4. Changes of velocity against Reynolds numbers for the case conducted on  $61^3$  meshes: (a)  $u(0, y, 0)$  and  $v(x, 0, 0)$  ; (b)  $w(0, 0, z)$  .

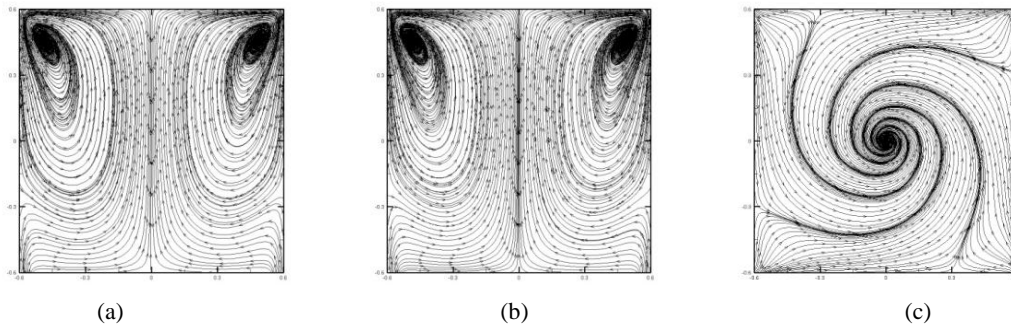


Figure 5. Computed secondary flow structure for the case of  $Re = 1000$  ; (a) computed pseudo-streamlines at the  $x = 0$  plane; (b) computed pseudo-streamlines at the  $y = 0$  plane; (c)  $z = 0$  at  $xy$  plane.

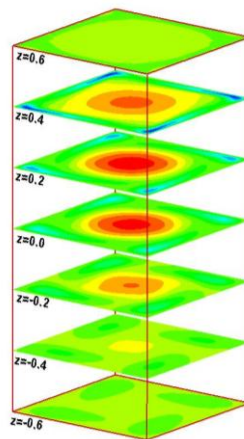


Figure 6. A three-dimensional plot for showing the positive  $\Omega$  velocity component (shaded area) in the cavity which has a disk angular speed  $\Omega$  in the corresponding Reynolds number of 1000.

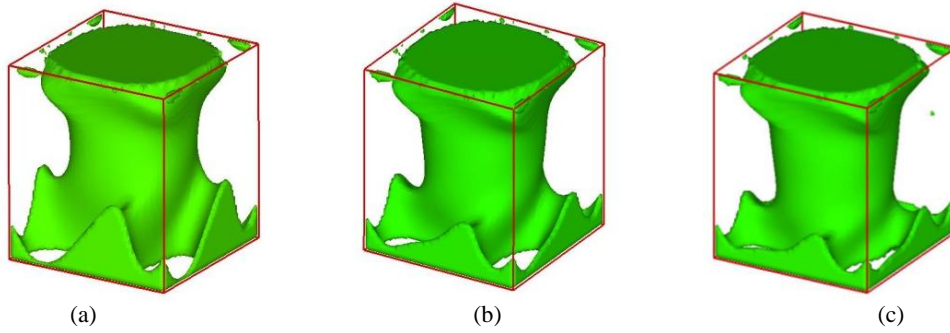


Figure 7. An illustration of the contour surface of  $w = 0$  in the cavity for the cases of (a)  $Re = 2000$  ; (b)  $Re = 3000$  ; (c)  $Re = 4000$  .

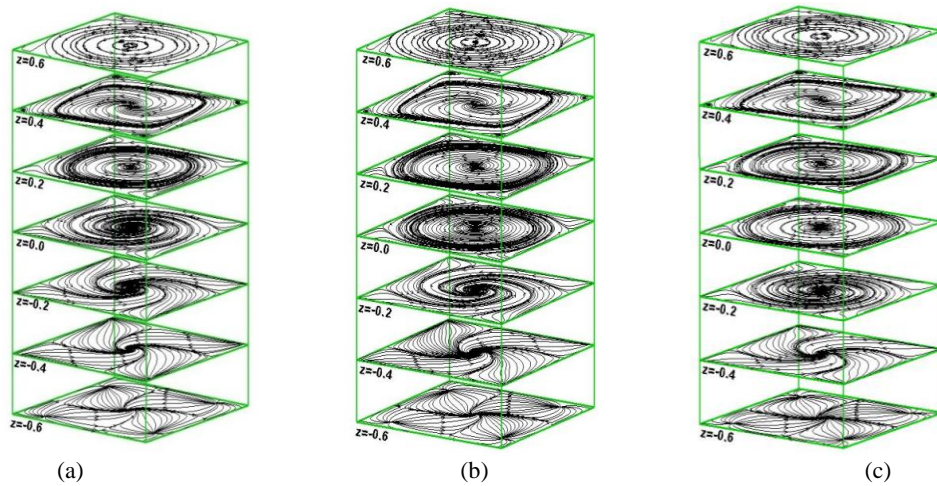


Figure 8. The computed pseudo-streamlines for the cases with different Reynolds numbers: (a)  $Re = 2000$  ; (b)  $Re = 3000$  ; (c)  $Re = 4000$  .

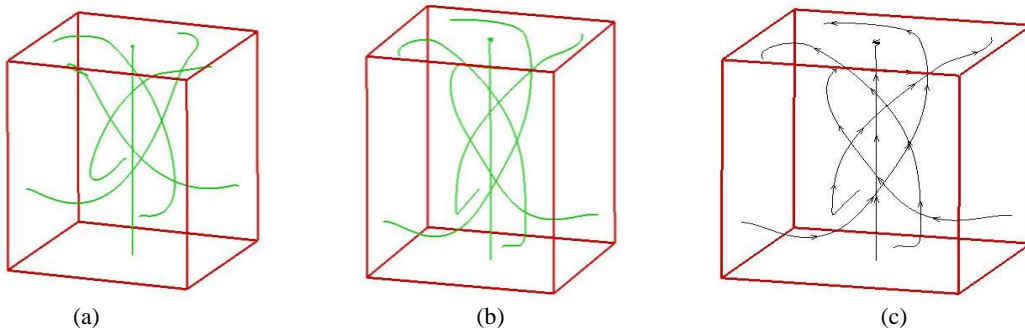


Figure 9. Detailed flow topologies in the marked area shown in Figure 7. (a)  $Re = 2000$  ; (b)  $Re = 3000$  ; (c)  $Re = 4000$  .